Simultaneous Raman Microspectroscopy and Fluorescence Imaging of Bone Mineralization in Living Zebrafish Larvae

M. Bennet,[†] A. Akiva,[‡] D. Faivre,[†] G. Malkinson,[§] K. Yaniv,[§] S. Abdelilah-Seyfried,[¶] P. Fratzl,[†] and A. Masic[†*]
[†]Department of Biomaterials, Max Planck Institute of Colloids and Interfaces, Potsdam, Germany; [‡]Department of Structural Biology, Weizmann Institute of Science, Rehovot, Israel; [§]Department of Biological Regulation, Weizmann Institute of Science, Rehovot, Israel; and [¶]Institute for Molecular Biology, Medizinische Hochschule Hannover, Hannover, Germany

ABSTRACT Confocal Raman microspectroscopy and fluorescence imaging are two well-established methods providing functional insight into the extracellular matrix and into living cells and tissues, respectively, down to single molecule detection. In living tissues, however, cells and extracellular matrix coexist and interact. To acquire information on this cell-matrix interaction, we developed a technique for colocalized, correlative multispectral tissue analysis by implementing high-sensitivity, wide-field fluorescence imaging on a confocal Raman microscope. As a proof of principle, we study early stages of bone formation in the zebrafish (*Danio rerio*) larvae because the zebrafish has emerged as a model organism to study vertebrate development. The newly formed bones were stained using a calcium fluorescent marker and the maturation process was imaged and chemically characterized in vivo. Results obtained from early stages of mineral deposition in the zebrafish fin bone unequivocally show the presence of hydrogen phosphate containing mineral phases in addition to the carbonated apatite mineral. The approach developed here opens significant opportunities in molecular imaging of metabolic activities, intracellular sensing, and trafficking as well as in vivo exploration of cell-tissue interfaces under (patho-)physiological conditions.

Received for publication 21 October 2013 and in final form 3 January 2014.

*Correspondence: masic@mpikg.mpg.de

M. Bennet and A. Akiva contributed equally to this work.

Understanding fundamental biological processes relies on probing intra- and extracellular environments, targeted delivery inside living cells and tissues, and real-time detection and imaging of chemical markers and biomolecules (1,2). Typically, information about molecules in cellular environments is obtained by fluorescence microscopy (3). This is a powerful imaging tool for localizing and imaging samples but requires fluorescent labels and markers and lacks capabilities for quantitative mapping of the chemical composition in complex systems. In this regard, confocal Raman spectroscopic imaging is becoming increasingly popular for label-free chemical detection, due to the inherent scattering nature of all biomolecules (4,5). However, confocal Raman imaging alone does not allow live, high-resolution imaging of larger regions of interest in complex biological tissues. Transcutaneous Raman spectroscopy has the potential as a tool for in vivo bone quality assessment (6), whereas the time- and space-resolved Raman spectroscopy allows the visualization in vivo of the distributions of molecular species in human and yeast cells (4,5,7). Here we developed a correlative Raman and fluorescence imaging method that combines the strengths and compensates for the shortcomings of each of these imaging modalities and allows studying in vivo processes in complex animal models such as zebrafish larvae. There are two main advantages of this approach over previous studies (8,9): low light intensity and high acquisition rate, making it well suited for real-time investigation of live samples.

Fig. 1, *a* and *b*, shows a schematic representation of the experimental setup and of the optical path, respectively. The two techniques are implemented on a commercially available Raman microscope body to perform simultaneously confocal Raman spectroscopy and wide-field fluorescence imaging (see the Supporting Material for details of components). Briefly, the multimodality of the setup is provided by a combination of dichroic mirrors (DM 1–3) and filters that at turns reflect or transmit the excitation and emission signals. This combination of optics allows simultaneous collection of fluorescence images (2560 × 2160 pixels at 30 fps) with excitation at 400 and 490 nm and spatially resolved Raman spectra with excitation at 633 nm.

As a proof of principle, we have studied the different mineral phases involved in bone formation of the zebrafish larvae. The bone development process involves the transport

Editor: Alan Grodzinsky.

http://dx.doi.org/10.1016/j.bpj.2014.01.002

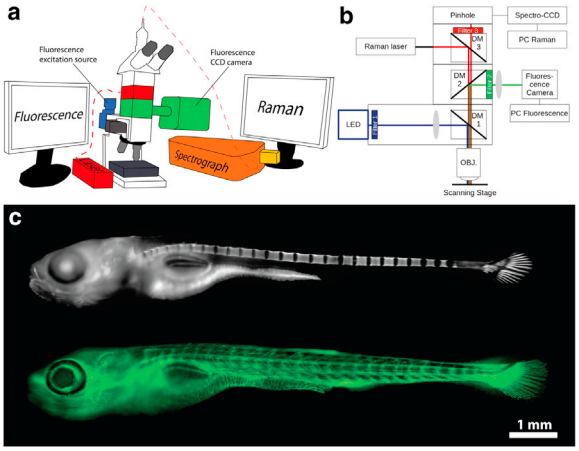

FIGURE 1 Fluorescence imaging of zebrafish larvae. (*a*) Cartoon of the experimental setup showing how the different modules are assembled onto the microscope for the simultaneous use of confocal Raman spectroscopy and fluorescence imaging. (*b*) Schematic representation of the optical path. (*c*) Fluorescence image of calcium-containing tissues, and fluids stained with calcein blue and excited at 400 nm (*top*). Endothelial cells of transgenic *tg*(*fli1:EGFP*)*y1* zebrafish excited at 490 nm (*bottom*).

of ions to specific cells (osteoblasts) that are responsible for the subsequent mineral formation and deposition. The mineral phase in these cells is a poorly characterized disordered calcium phosphate (10–12). The mineral-bearing intracellular vesicles release their content into the extracellular collagen fibrils, where the mineral subsequently crystallizes as carbonated hydroxyapatite (13). Very little is known about the phase transformations the mineral undergoes after the deposition into the collagen matrix in vivo. Raman spectroscopy studies of bone tissue in organ cultures evidenced that the inorganic mineral deposition proceeds through transient intermediates including octacalcium phosphate-like (OCP) minerals (14).

To assess the feasibility of imaging a vertebrate organism, fluorescence images of an entire zebrafish larva (Fig. 1 *c*) were acquired with the correlative fluorescence-Raman setup. The two images in Fig. 1 *c* were composed by merging several low-magnification (10×) fluorescence images. Larvae of transgenic zebrafish *Tg*(*fli:EGFP*); *nac* mutants (albino fish) expressing EGFP in the cytoplasm of endothelial cells was used. The newly formed bones were stained by soaking the live embryo noninvasively in the calcium markers calcein blue 0.2% wt or calcein green 0.2% wt.

The calcein blue marker is excited at 400 nm. It is labeling bones and can be also detected as a fluorescent marker not associated with formed bones (e.g., stomach) (Fig. 1 *c*, *top*). At 490 nm, calcein green and endothelial cells within blood vessels expressing EGFP are excited (Fig. 1 *c*, *bottom*). Because EGFP and calcein blue have significantly different excitation and emissions spectra, dual staining with calcein blue (as a mineral marker) and EGFP allows fast-switching dual-wavelength fluorescence imaging. Furthermore, because the spectra of the calcium markers and EGFP do not extend beyond the Raman laser, these fluorophores are appropriate candidates for experiments requiring Raman and fluorescence imaging. The dual-excitation offers the capability of mapping several tissues in a single experiment at the video rate. This, in principle, could be used to probe different parameters of the microenvironment (e.g., pH (15), temperature (16), viscosity (17), and calcium concentration (18)) using wavelength-ratiometric fluorescence imaging which, in correlation with confocal Raman spectroscopy, could open new strategies in studies of the microenvironmental properties in living tissues.

The fin rays of zebrafish are a simple, growing bone-model system, in which the fins are gradually mineralized within spatially resolved regions (19). Raman spectroscopy revealed details of the calcein green-stained fin where new bone is deposited (Fig. 2). In Fig. 2 *a*, a fluorescence image of a zebrafish larva analogous to the top image in Fig. 1 *c* is shown. The right inset in Fig. 3 *b* shows higher-magnification (60× water-immersion objective) details of the calcein green-stained fin typical of newly deposited bone. Raman spectra of progressively mineralized bone tissue were acquired within representative regions (Fig. 2 *b*; numbered 1–4). The spectra exhibit characteristic bands that can be assigned to the organic protein extracellular matrix (amide I, amide III, Phe, C-H, etc.) and the inorganic mineral content (v_1, v_2, v_4 of PO_4^{3-}).

The analyses of the orientation-independent v_2 phosphate band revealed a clear drop in the mineral content based on the intensity integral (*left inset* in Fig. 2 *b*). Assuming that the spectrum collected in region 4 contains only organic matrix (very small phosphate-related peaks) and by subtracting it from the spectrum of mineral-rich bone region (spectrum 1, proximal part of the tail bone), spectral features of only the mineral phase can be plotted (*black line*). In addition to the phosphate (PO_4^{3-}) and carbonate (CO_3^{2-}) bands assignable to the carbonated apatite phase characteristic of the more mature bone mineral, several peaks related to the hydrogen phosphate (HPO_4^{2-}) species can be clearly distinguished.

The HPO_4^{2-} peaks are characteristic of the OCP mineral phase that has been postulated, together with amorphous calcium phosphate, as an intermediate mineral phase in the process of bone maturation (10,13,14,20), but never observed directly in living animals. Our findings show in vivo potential of the correlative setup envisioned by Crane et al. (14) and confirm that the mineral maturation indeed proceeds through an OCP-like mineral phase. Further analysis of the mineral spectrum in Fig. 2 *b* reveals an extremely broad band in the region 800–1100 cm^{-1}. This envelope can be related to hydrogenated phosphate species typical of amorphous calcium phosphate precipitated in an acidic environment (see Fig. S1 in the Supporting Material), suggesting that this phase is also contributing to the maturation process.

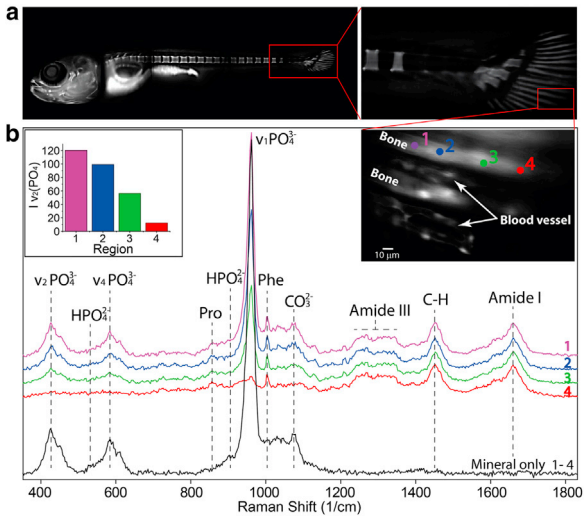

FIGURE 2 Correlative fluorescence-Raman imaging of zebrafish fin bone maturation. (*a*) Low-resolution (10×) fluorescence image of zebrafish stained with calcein green, with high-resolution (60×) details (*right inset* in panel *b*) of a representative fin ray region where Raman spectra (*b*) of progressively mineralized bone tissue were acquired (numbered 1–4). (*Left inset* in panel *b*) Integral of the orientation independent mineral band (v_2) where a clear drop of the mineral content can be observed.

In conclusion, the methodology developed here allows for unprecedented chemical characterization of fluorescently-labeled biological tissues in vivo. The approach is suitable for long-term in vivo characterization of zebrafish bone mineralization under (patho-)physiological conditions. Furthermore, the setup can be upgraded to host other advance fluorescence imaging techniques such as super-resolution microscopy (e.g., photoactivated localization microscopy), two-photon excitation, and Forster resonance energy transfer or fluorescence lifetime imaging microscopy, and be applied on both in vivo and in vitro specimens. This opens significant opportunities in molecular imaging of metabolic activities, intracellular sensing, and trafficking as well as in vivo exploration of cell-tissue interfaces.

SUPPORTING MATERIAL

Materials and Methods (Fish Husbandry, Sample Preparation, Correlative Fluorescence-Raman Setup), one table, and one figure are available at http://www.biophysj.org/biophysj/supplemental/S0006-3495(14)00058-7.

ACKNOWLEDGMENTS

We thank Professors Lia Addadi and Steve Weiner and Dr. Wouter Habraken for discussions.

This research was supported by a German Research Foundation grant, within the framework of the Deutsch-Israelische Projektkooperation. P.F. is grateful for support by the German Science Foundation within the Leibniz-Award. D.F. is supported by a starting grant from the European Research Council (Project MB2, No. 256915). G.M. is supported by the Israel Cancer Research Foundation postdoctoral fellowship. K.Y. is the incumbent of the Louis and Ida Rich Career Development Chair, and is supported in part by the Marie Curie Actions-International Reintegration grant (No. FP7-PEOPLE-2009-RG 256393). S.A.-S. is supported by a Heisenberg-Professorship of the German Science Foundation (No. SE2016/9-2).

REFERENCES and FOOTNOTES

1. Watson, P., A. T. Jones, and D. J. Stephens. 2005. Intracellular trafficking pathways and drug delivery: fluorescence imaging of living and fixed cells. *Adv. Drug Deliv. Rev.* 57:43–61.
2. Skirtach, A. G., A. Muñoz Javier, …, G. B. Sukhorukov. 2006. Laser-induced release of encapsulated materials inside living cells. *Angew. Chem. Int. Ed. Engl.* 45:4612–4617.
3. Lackowitz, J. 2006. Principles of Fluorescence Spectroscopy. Springer, New York.
4. Klein, K., A. M. Gigler, …, J. Schlegel. 2012. Label-free live-cell imaging with confocal Raman microscopy. *Biophys. J.* 102:360–368.
5. Matthäus, C., T. Chernenko, …, M. Diem. 2007. Label-free detection of mitochondrial distribution in cells by nonresonant Raman microspectroscopy. *Biophys. J.* 93:668–673.
6. Schulmerich, M. V., K. A. Dooley, …, S. A. Goldstein. 2006. Transcutaneous fiber optic Raman spectroscopy of bone using annular illumination and a circular array of collection fibers. *J. Biomed. Opt.* 11:060502.
7. Huang, Y. S., T. Karashima, …, H. O. Hamaguchi. 2005. Molecular-level investigation of the structure, transformation, and bioactivity of single living fission yeast cells by time- and space-resolved Raman spectroscopy. *Biochemistry.* 44:10009–10019.
8. Uzunbajakava, N., and C. Otto. 2003. Combined Raman and continuous-wave-excited two-photon fluorescence cell imaging. *Opt. Lett.* 28:2073–2075.
9. Engel, S. R., P. Koch, …, A. Leipertz. 2009. Simultaneous laser-induced fluorescence and Raman imaging inside a hydrogen engine. *Appl. Opt.* 48:6643–6650.
10. Mahamid, J., B. Aichmayer, …, L. Addadi. 2010. Mapping amorphous calcium phosphate transformation into crystalline mineral from the cell to the bone in zebrafish fin rays. *Proc. Natl. Acad. Sci. USA.* 107:6316–6321.
11. Weiner, S. 2006. Transient precursor strategy in mineral formation of bone. *Bone.* 39:431–433.
12. Olszta, M. J., X. G. Cheng, …, L. B. Gower. 2007. Bone structure and formation: a new perspective. *Mater. Sci. Eng. Rep.* 58:77–116.
13. Mahamid, J., A. Sharir, …, S. Weiner. 2011. Bone mineralization proceeds through intracellular calcium phosphate loaded vesicles: a cryo-electron microscopy study. *J. Struct. Biol.* 174:527–535.
14. Crane, N. J., V. Popescu, …, M. A. Ignelzi, Jr. 2006. Raman spectroscopic evidence for octacalcium phosphate and other transient mineral species deposited during intramembranous mineralization. *Bone.* 39:434–442.
15. Rodo, A. P., L. Vachova, and Z. Palkova. 2012. In vivo determination of organellar pH using a universal wavelength-based confocal microscopy approach. *PLoS One.* http://dx.doi.org/10.1371/journal.pone.0033229.
16. Barilero, T., T. Le Saux, …, L. Jullien. 2009. Fluorescent thermometers for dual-emission-wavelength measurements: molecular engineering and application to thermal imaging in a microsystem. *Anal. Chem.* 81:7988–8000.
17. Luby-Phelps, K., S. Mujumdar, …, A. S. Waggoner. 1993. A novel fluorescence ratiometric method confirms the low solvent viscosity of the cytoplasm. *Biophys. J.* 65:236–242.
18. Neher, E., and G. J. Augustine. 1992. Calcium gradients and buffers in bovine chromaffin cells. *J. Physiol.* 450:273–301.
19. Becerra, J., G. S. Montes, …, L. C. Junqueira. 1983. Structure of the tail fin in teleosts. *Cell Tissue Res.* 230:127–137.
20. Popescu, V., N. J. Crane, …, P. Steenhuis. 2005. Octacalcium phosphate (OCP) and other transient mineral species are observed in mouse sutures during normal development and craniosynostosis. *J. Bone Miner. Res.* 20:S106.

DATA S1: SUPPLEMENTAL MATERIALS

Simultaneous Raman microspectroscopy and fluorescence imaging of bone mineralization in living zebrafish larvae

M. Bennet*°, A. Akiva[†]°, D. Faivre*,G. Malkinson[‡], K. Yaniv[‡], S. Abdelilah-Seyfried[¶], P. Fratzl*, A. Masic*[©]

* Dept. of Biomaterials, Max Planck Institute of Colloids and Interfaces, Potsdam, Germany; [†]Dept. of Structural Biology, Weizmann Institute of Science, Rehovot, Israel; [‡] Dept. of Biological Regulation, Weizmann Institute of Science, Rehovot, Israel; [¶]Institute for Molecular Biology, Medizinische Hochschule Hannover, Hannover, Germany. °These authors contributed equally to this work.

[©]Correspondence: masic@mpikg.mpg.de

A. SUPPLEMENTAL MATERIALS AND METHODS

Fish husbandry: Zebrafish were raised according to standard methods(1, 2), and handled according to the guidelines of the Weizmann Institute Animal Care and Use Committee. Handling of zebrafish was also done in compliance with German and Berlin state law, carefully monitored by the local authority for animal protection (Lageso, Berlin-Brandenburg, Germany). The following fish strains were used: *Tg(fli:EGFP)*^{y1}(3), *nac* mutants(4).

Sample preparation: In order to monitor zebrafish bone formation *in vivo*, a calcein green fluorescent marker [CAS number 1461-15-0 Sigma-Aldrich] and calcein blue [CAS number 54375-47-2 Sigma-Aldrich] were used. Calcein binds to free calcium ion and stain newly formed bones. To visualize and analyze the mineral content of newly formed bones, we used 20-27 days post fertilization (dpf) zebrafish. The fish were immersed 30 minutes in calcein solution (0.2% wt)(5) with calcein green, or overnight in calcein blue, and then rinsed in fresh water three times in order to allow diffusion of the free calcein. After rinsing in water, the fish were anesthetized in 0.16% tricaine-methanesulfonate (MS222) solution, and mounted on depression slides using methyl-cellulose [CAS M0387 Sigma-Aldrich (6%)] or low-melt agarose (9012-36-6) before non-invasive imaging. This protocol allows for visualization of bones and endothelial cells with two different green fluorescence markers or green and blue fluorescence markers within the same animal, enabling identification of the region of interest, prior to the Raman analysis.

Correlative fluorescence-Raman setup: The setup is built on the commercially available confocal Raman microscope (alpha300, WITec, Ulm, Germany) equipped with a Helium Neon (HeNe) (633 nm) laser excitation and piezoscanner (P-500, Physik Instrumente, Karlsruhe, Germany). The spectra were acquired with a thermoelectrically cooled CCD detector (DU401A-

BV, Andor, UK) placed behind a grating (600 g mm^{-1}) spectrograph (UHTS 300; WITec, Ulm, Germany) with a spectral resolution of 3 cm^{-1}. The laser beam was focused through a 10× (Nikon, NA = 0.2) and 60× water immersion (Nikon, NA=1.0) microscope objectives. The ScanCtrlSpectroscopyPlus software (version 1.38, Witec) was used for measurement and WITec Project Plus (version 2.10, Witec) for spectra processing. The Raman signal is spectrally filtered by a longpass filter (filter 3).

The implementation of the fluorescence modality relies on the substitution of some of the original optics, integration of excitation light in addition to the white illumination light, and the addition of a module in the imaging arm. Details of the changes made are shown in Fig.1 and summarized in Table 1. The excitation for the fluorescence is held in the illumination port at the back of the microscope and spectrally selected by the filter positioned in the filter holder (filter 1). The excitation light is reflected by the dichroic mirror (DM1) and the sample illuminated by the objective in place. The signal from the sample is collected in the epifluorescence mode, transmitted through the dichroic mirror (DM1) and reflected by the second dichroic mirror (DM2) placed in the first module of the microscope imaging arm. The signal is spectrally filtered at the desired wavelength (filter 2) and imaged onto a fluorescence camera by an achromatic doublet lens. Because DM1 and DM2 transmit the Raman laser (red to deep-infrared) and the scattered light in the Stoke region of the spectra, the setup allows simultaneous live visualization in the fluorescence mode and live collection of the Raman spectra. The dichroic mirror (DM1) and excitation filter (filter 1) allow a choice for the excitation wavelength for the fluorescence. This can be made at 400 or 490 nm, without modifying the current optical setting. These two wavelengths can excite a major part of the fluorescent markers and proteins used in traditional fluorescence imaging. Furthermore, the setup can be easily tailored to other wavelengths.

Table 1: Details of the components added to the microscope.

Added Components	**Details**
LED	pE-100, 400 or 490 nm,CoolLED
Filter 1	F69-390, HC Tripleband Exciter 482/587, AHF
Dichroic Mirror 1 (DM1)	F38-495, Strahlenteiler HC BS 495 AHF
Dichroic Mirror 2 (DM2)	F48-567, Strahlenteiler T 565 LPXR AHF
Filter 2	F67-446, HC Tripleband Sperrfilter 446/532/646, AHF
Lens	Achromatic Doublet, Imaging Lens, Thorlabs
Fluorescence Camera	NeoSCMOS, Andor

B. SUPPLEMENTAL FIGURE

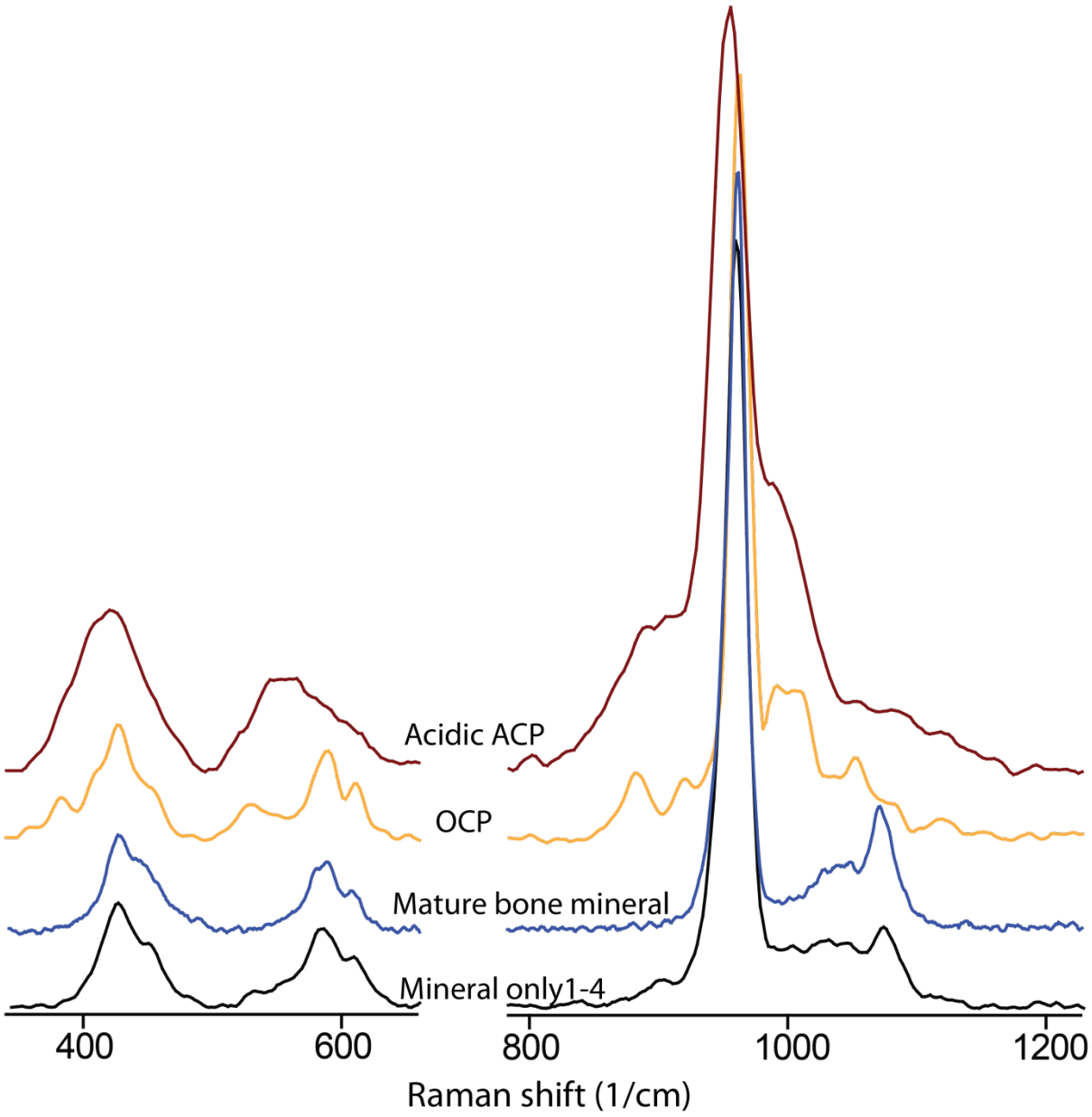

Figure S1: Reference spectra of acidic amorphous calcium phosphate (acidic ACP), octacalcium phosphate (OCP), mature zebrafish mineral, and zebrafish bone mineral phase shown in Fig. 3b.

References

1. Yaniv, K., S. Isogai, D. Castranova, L. Dye, J. Hitomi, and B. M. Weinstein. 2006. Live imaging of lymphatic development in the zebrafish. Nat. Med. 12:711-716.

2. Westerfield, M. 2000. The Zebrafish Book. A Guide for the Laboratory Use of Zebrafish (Danio rerio). University of Oregon Press, Eugene

3. Lawson, N. D., and B. M. Weinstein. 2002. In vivo imaging of embryonic vascular development using transgenic zebrafish. Dev. Biol. 248:307-318

4. Lister, J. A., C. P. Robertson, T. Lepage, S. L. Johnson, and D. W. Raible. 1999. Nacre encodes a zebrafish microphthalmia-related protein that regulates neural-crest-derived pigment cell fate. . Development 126:3757-3767.

5. Du, S. J., V. Frenkel, G. Kindschi, and Y. Zohar. 2001. Visualizing normal and defective bone development in zebrafish embryos using the fluorescent chromophore calcein. Dev. Biol. 238:239-246.